Probabilistic analysis of seepage for internal stability of earth embankments

Liu, Kang; Vardon, Philip J.; Hicks, Michael A.

Important note
To cite this publication, please use the final published version (if applicable).
Please check the document version above.

Environmental Geotechnics

ice Publishing

Probabilistic analysis of seepage for internal stability of earth embankments

[1] **Kang Liu** BSc, MSc, PhD
Researcher, Geo-engineering Section, Faculty of Civil Engineering and Geosciences, Delft University of Technology, Delft, the Netherlands; Now Assistant Professor, School of Civil and Hydraulic Engineering, Hefei University of Technology, Hefei, Anhui, China

[2] **Philip J. Vardon** MEng, PhD
Associate Professor, Geo-engineering Section, Faculty of Civil Engineering and Geosciences, Delft University of Technology, Delft, the Netherlands (corresponding author: p.j.vardon@tudelft.nl)
(Orcid:0000-0001-5614-6592)

[3] **Michael A. Hicks** BSc, PhD
Professor, Geo-engineering Section, Faculty of Civil Engineering and Geosciences, Delft University of Technology, Delft, the Netherlands
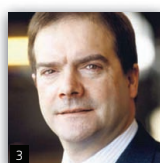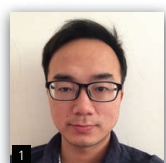
Internal erosion, or piping, has been attributed as a major cause of dam and embankment failures. Most prediction models for predicting piping use the hydraulic gradient between the upstream and downstream water levels as an indicator. No explicit consideration is made regarding preferential pathways, although piping usually initiates from a discrete downstream location. The local seepage velocity is investigated here through stochastic seepage analysis incorporating consideration of soil heterogeneity. The results show that when the coefficient of variation of hydraulic conductivity is small, the location of the maximum local velocity is typically near the downstream toe of the embankment, as for a deterministic analysis. In contrast, increasing the coefficient of variation scatters the possible locations of the maximum local velocity. The heterogeneity of hydraulic conductivity also leads to an increase in the average exit hydraulic gradient, as well as having a significant influence on the global kinetic energy and kinetic energy distribution.

Notation

A	total area of the cross-section
A_p	area of the voids in the cross-section
COV_k	coefficient of variation of hydraulic conductivity
E_g	global kinetic energy of the water
$E_{g,homo}$	E_g when the foundation is homogeneous
E_l	local kinetic energy of the water
FOS	factor of safety
H_c	hydraulic difference across the structure
h	hydraulic head
i_c	critical exit gradient
k	hydraulic conductivity
k_x	hydraulic conductivity in the x direction
k_y	hydraulic conductivity in the y direction
L	length of the seepage path
M_f	mass of fluid
n	porosity
p	pore pressure
q	discharge
V	volume of soil
v	Darcy flow velocity
v_c	critical local velocity
v_s	pore seepage velocity
v_{maxd}	deterministic maximum local velocity
v_{max}^b	maximum local velocity in the hatched area
x, y	Cartesian coordinates
z	elevation
γ_w	unit weight of water
θ_h	horizontal scale of fluctuation of hydraulic conductivity
θ_k	scale of fluctuation of hydraulic conductivity
θ_v	vertical scale of fluctuation of hydraulic conductivity
μ_k	mean of hydraulic conductivity
$\mu_{v_{max}}$	mean of maximum local velocity
ξ	degree of anisotropy of the heterogeneity
ρ_s	density of soil solid
ρ_w	density of water
σ_k	standard deviation of hydraulic conductivity
$\sigma_{v_{max}}$	standard deviation of maximum local velocity

Introduction

Piping has been attributed as a major cause of dam failures, with about half of all failures being due to piping (Foster *et al.*, 2000). It usually happens in the presence of a water barrier, with a high water level on one side and a low level on the other. The hydraulic head difference induces a water flow in the structure (Sellmeijer and Koenders, 1991), and when the flow reaches a critical rate, it starts to erode soil particles from the downstream surface (piping initiation). Subsequently, the internal erosion progresses in the upstream direction and a piping channel or slit is formed (piping development). Finally, if the piping process does not come to a

Environmental Geotechnics
Volume 6 Issue EG5

Probabilistic analysis of seepage for
internal stability of earth embankments
Liu, Vardon and Hicks

halt, the erosion channels progress to the upstream surface, and then, the erosion through the channels can accelerate significantly and the water barrier can be 'undermined' and collapse.

Accurate analysis of whether piping is going to happen is essential in the design and management of water barriers. Figure 1 simply illustrates the piping process: Figure 1(a) shows the initiation of piping, where heaving leads to a discrete initialisation of the pipe, often seen in practice as a sand boil; Figure 1(b) shows the piping development, where the material is able to be continually transported through the pipe and the pipe grows in length. Current models for predicting piping initiation and development are Bligh's model, Lane's model and Sellmeijer's model (Bligh, 1910; Lane, 1935; Sellmeijer and Koenders, 1991). The first two are empirical, whereas the last one is conceptual (Sellmeijer, 2006). However, all these models use hydraulic gradient as an indicator of the state governing piping occurrence. Bligh's model relates the hydraulic head difference across the structure, H_c, to the length of the seepage path, L. The critical value of the ratio H_c/L is related to the soil type. Lane's model is similar to Bligh's model, except that it accounts for the horizontal and vertical seepage lengths separately, in order to account for the influence of different permeabilities in the horizontal and vertical directions. In Sellmeijer's model, the critical value of H_c/L is also related to additional factors, which include the sand bedding angle, the sand particle size and the geometry of the water barrier. However, piping normally initiates from a very local downstream position. Therefore, local behaviour close to the downstream ground surface is important, and local behaviour is strongly related to the inherent heterogeneity of the soil.

Recent research has illustrated that hydraulic velocity is an indicator of piping potential (Sivakumar Babu and Vasudevan, 2008) and can be an improvement to using simply the hydraulic gradient (Richards and Reddy, 2012). The velocity is a function of hydraulic conductivity and hydraulic gradient. However, due to the heterogeneity of hydraulic conductivity, the hydraulic gradient across the entire structure cannot be seen as directly proportional to the local velocity; therefore, the local velocity distribution within the domain is of interest and forms the main focus of this paper.

This paper investigates the local velocity distribution under an earth embankment, induced by the spatial variability of the foundation hydraulic conductivity, and considers its influence on the potential for piping. The piping process itself is not modelled and would require a large deformation model (e.g. Wang *et al.*, 2016). The section headed 'Stochastic seepage analysis' introduces stochastic seepage computed by the random finite-
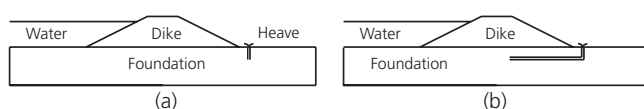
element (FE) method (RFEM). The section headed 'Probabilistic analysis of seepage in and under an embankment' presents stochastic analyses of velocity distribution, including a parametric study relating to the statistics of hydraulic conductivity. The section headed 'Analysis of local velocity distribution with reference to piping' includes a discussion on the influence of soil heterogeneity on piping potential. The section headed 'Exit gradient related to piping initiation' calculates the exit velocity related to the piping initiation. The section headed 'Influence of heterogeneity on the kinetic energy of seepage' investigates the kinetic energy distribution in the whole domain under the influence of heterogeneity.

Stochastic seepage analysis

The local velocity distribution is computed in a seepage analysis, and, herein, an idealised two-dimensional (2D) steady-state seepage problem with constant boundary conditions has been analysed. The governing equation of steady-state groundwater flow in two dimensions is as follows, with the deformation of the domain and compressibility of water being neglected (Smith *et al.*, 2013).

1.
$$\frac{\partial}{\partial x}\left(k_x \frac{\partial h}{\partial x}\right) + \frac{\partial}{\partial y}\left(k_y \frac{\partial h}{\partial y}\right) = 0$$

where $h = z + p/\gamma_w$ is the hydraulic head, in which z is the elevation; p is the pore pressure; γ_w is the unit weight of water; and k_x and k_y are the hydraulic conductivities in the x and y directions, respectively.

Over the domain, the hydraulic conductivity is taken as a spatially random variable so that a stochastic seepage analysis can be undertaken. The hydraulic conductivity is log-normally distributed (Griffiths and Fenton, 1993), and RFEM is applied to incorporate the uncertainty existing in the hydraulic conductivity. Griffiths and Fenton (1993) first applied RFEM to stochastic seepage in the foundation of a water-retaining structure. Since then, a series of stochastic seepage studies have been undertaken using this method. Some have focused on the seepage itself (Fenton and Griffiths, 1996), whereas others have studied the influence of stochastic seepage on slope or embankment stability (Le *et al.*, 2012). RFEM is the combination of a random field generator, such as one based on local average subdivision (LAS) (Fenton and Vanmarcke, 1990), to create 'random fields' of material parameters, the finite-element method (FEM) and the Monte Carlo method. Generally speaking, the stochastic seepage can be realised in three steps. First, LAS or some other similar technique is used to generate a random field of hydraulic conductivity based on the statistical values of hydraulic conductivity – that is, the mean μ_k and standard deviation σ_k and the scale of fluctuation θ_k reflecting the spatial correlation of hydraulic conductivity at different locations. Then, FEM is used to compute the pore pressure, seepage velocity and so on. Finally, the process is repeated multiple times as part of a Monte Carlo simulation (Hicks and Samy, 2004). To reduce uncertainty in stochastic

Figure 1. Sketch of piping initiation (a) and piping development (b)

Environmental Geotechnics
Volume 6 Issue EG5

Probabilistic analysis of seepage for
internal stability of earth embankments
Liu, Vardon and Hicks

analyses, inverse modelling based on data assimilation can be used (Liu, 2017; Liu *et al.*, 2017; Vardon *et al.*, 2016) and/or random fields conditioned to site-specific data – for example, cone penetration tests – utilising techniques such as Kriging (e.g. Li *et al.*, 2016; Lloret-Cabot *et al.*, 2012).

In this study, a fixed FE mesh is used to solve Equation 1 and also prescribed hydraulic head (Dirichlet) boundary conditions. However, in this saturated unconfined flow problem, there are unknown boundary conditions, which are the position of the phreatic surface and the exit point on the downstream surface of the embankment. During the computation, an iterative process is adopted to determine the exact positions of the exit point and phreatic surface (Chapuis and Aubertin, 2001; Chapuis *et al.*, 2001). An outer iteration loop is used to determine the position of the exit point, and an inner iteration loop is used to determine the position of the phreatic surface. The outer iteration stops when the nodes on the downstream surface of the embankment which are above the exit point have no positive pore water pressure. The inner iteration stops when the hydraulic head at every node converges.

In the fixed-mesh method, the hydraulic conductivity at each Gauss point in the domain is analysed according to the pore pressure p. When $p \geq 0$, the hydraulic conductivity is equal to k and when $p < 0$, the hydraulic conductivity is 0 (Bathe and Khoshgoftaar, 1979). Hence, the elements in the dry region are effectively removed from the computation, while those in the wet region remain active.

Probabilistic analysis of seepage in and under an embankment

The example 2D steady-state seepage problem analysed herein is shown in Figure 2. A 4 m high earth embankment is constructed on a 5 m deep foundation overlying a firm base. The widths of the embankment crest and foundation are 4 and 40 m, respectively. The upstream and downstream side-slopes are both 1:2, and the upstream and downstream water levels are 4 and 0 m, respectively (where the coordinate origin is at the top left corner of the foundation). For simplicity, the embankment is considered to be homogeneous and only the foundation is heterogeneous. This is also because the main focus is on the role of the foundation in the seepage process. Although the geometries of the embankment and foundation are symmetrical, the problem is not symmetrical because of the boundary conditions and the heterogeneous hydraulic conductivity profile in the foundation.

The hydraulic conductivity of the embankment and mean hydraulic conductivity of the foundation are both chosen to be 10^{-6} m/s, consistent with a sandy material. Duncan (2000) suggested that the coefficient of variation ($COV_k = \sigma_k/\mu_k$) of hydraulic conductivity of saturated clay is 68–90%, whereas Zhu *et al.* (2013) suggested that for saturated sand, it is 60–100%. However, in order to get a detailed overview of the influence of the coefficient of variation of hydraulic conductivity on the statistical characteristics of the maximum local velocity, a much wider range of COV_k was used – that is, $COV_k = \sigma_k/\mu_k = 0.1, 0.5, 1.0, 2.0, 3.0, 4.0, 5.0$ and 6.0. The degrees of anisotropy of the heterogeneity considered were $\xi = \theta_h/\theta_v = 1, 8$ and 20 (where the subscripts h and v refer to the horizontal and vertical directions, respectively), and the vertical scale of fluctuation has been fixed at $\theta_v = 1.0$ m. The mesh for the finite element (FE) computation uses four-node quadrilateral elements of size 0.5 m by 0.5 m, except for some distorted elements, to model the upstream and downstream slope surfaces. The cell size in the random field generation is half of the FE mesh size in each direction, so that each of the four integration points in every FE has a different value from the random field.

Figure 3 shows typical random fields of the hydraulic conductivity k for two degrees of anisotropy, in which the darker zones represent lower values of k. Figure 3 shows that when the degree of anisotropy increases (for a given value of θ_v), the local variation of the hydraulic conductivity is not as great. Of course, when the COV_k increases, the range of the hydraulic conductivity also increases.

In each realisation, the velocity was calculated at the four integration points of each element, and the maximum local velocity within the foundation was identified. The statistical results of the
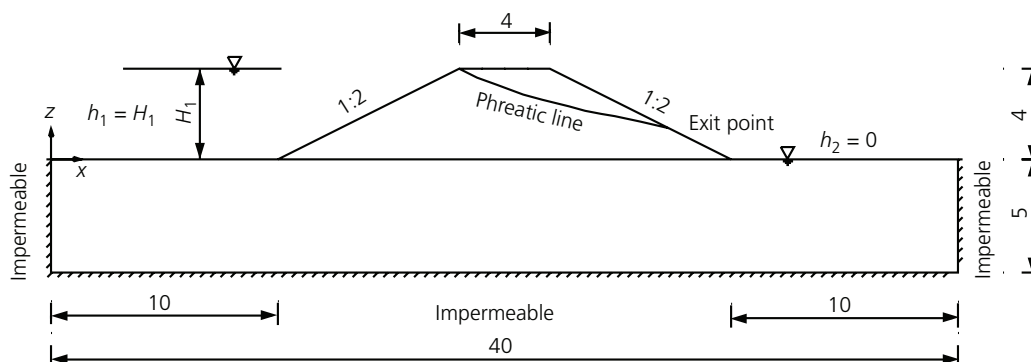

Figure 2. Geometry of the embankment and foundation (dimensions in metres)

Environmental Geotechnics
Volume 6 Issue EG5

Probabilistic analysis of seepage for
internal stability of earth embankments
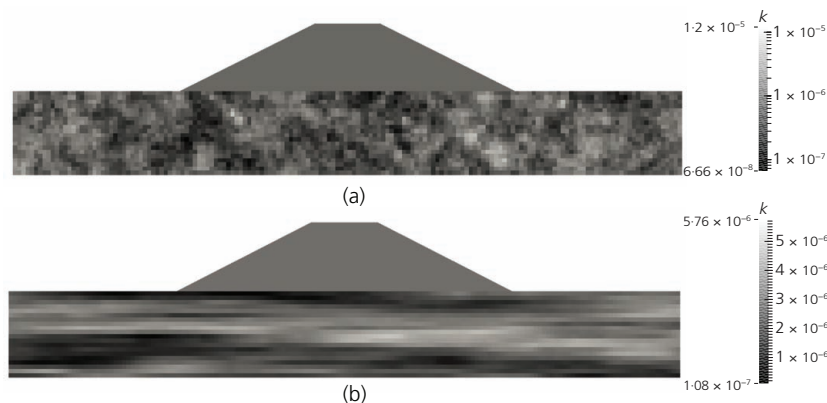Liu, Vardon and Hicks

Figure 3. Example of random fields for different hydraulic conductivity statistics (unit: metres per second): (a) typical random field for $COV_k = 1 \cdot 0$ and $\xi = 1$ and (b) typical random field for $COV_k = 1 \cdot 0$ and $\xi = 20$

velocity distributions for 500 and 1000 realisations were compared for selected values of the coefficients of variation and degrees of anisotropy (i.e. $COV_k = 1 \cdot 0$, $6 \cdot 0$ and $\xi = 1$, 8, 20), with little difference being found in the results of the mean and standard deviation of the maximum velocity (see Table 1). Therefore, 500 realisations were deemed adequate to get reasonable results for the complete range of input statistics considered. Figure 4 illustrates the close agreement between using 500 and 1000 realisations, by showing example histograms of the maximum velocity, in which the continuous lines represent the fitted log-normal distributions. It is seen that the log-normal distributions fit the histograms reasonably well. Figures 5 and 6 show the computed velocity distributions for two typical realisations.

The mean $\mu_{v_{max}}$ and standard deviation $\sigma_{v_{max}}$ of the maximum local velocity are influenced by the statistical values of the foundation hydraulic conductivity. Figures 7 and 8 show that $\mu_{v_{max}}$ and $\sigma_{v_{max}}$ are functions of the coefficient of variation of the foundation hydraulic conductivity COV_k. In Figure 7, $\mu_{v_{max}}$ is not sensitive to ξ. Moreover, the value of $\mu_{v_{max}}$ is larger than the deterministic maximum local velocity, $v_{maxd} = 6 \cdot 86 \times 10^{-7}$ m/s, for all values of COV_k considered. This is due to the water preferring a path with a low resistance to flow through and that, under the same hydraulic gradient, the lower-resistance path causes a higher velocity. In a heterogeneous domain, the local variation of the hydraulic conductivity is significant compared to the uniform hydraulic conductivity in a homogeneous domain

(based on the mean). In Figure 7, $\mu_{v_{max}}$ initially increases with increasing COV_k, after which a slight decrease occurs. The velocity is a function of the hydraulic conductivity and hydraulic gradient. It can be seen from Figure 9 that due to the log-normal statistics, the hydraulic conductivity distribution curves shift to the left with an increasing σ_k (indicated by an increasing COV_k). When σ_k is relatively small – that is, $COV_k < 2$, the distribution also becomes wider with an increase in σ_k. This means that the maximum value of the hydraulic conductivity increases, whereas the minimum value decreases. The increasing range of possible values for the hydraulic conductivity could cause the local hydraulic gradient to become larger, and this could be the reason for the local increase of velocity. However, when COV_k is greater than $3 \cdot 0$, the distribution curves become narrower. It can be seen from Figure 9 that the maximum value of the hydraulic conductivity also starts to decrease at higher values of COV_k which may be the reason for the slight decrease in $\mu_{v_{max}}$ in Figure 7. Figure 8 shows that $\sigma_{v_{max}}$ increases monotonically with an increase in COV_k and that, for the same value of COV_k, $\sigma_{v_{max}}$ increases with an increase in ξ.

Analysis of local velocity distribution with reference to piping
The previous section has analysed the general features of the local velocity distribution due to the spatial variability of the foundation hydraulic conductivity – for example, the distribution of maximum local velocity based on 500 realisations and its sensitivity to

Table 1. Mean and standard deviation of maximum velocities based on different numbers of realisations for different COV_k and ξ values

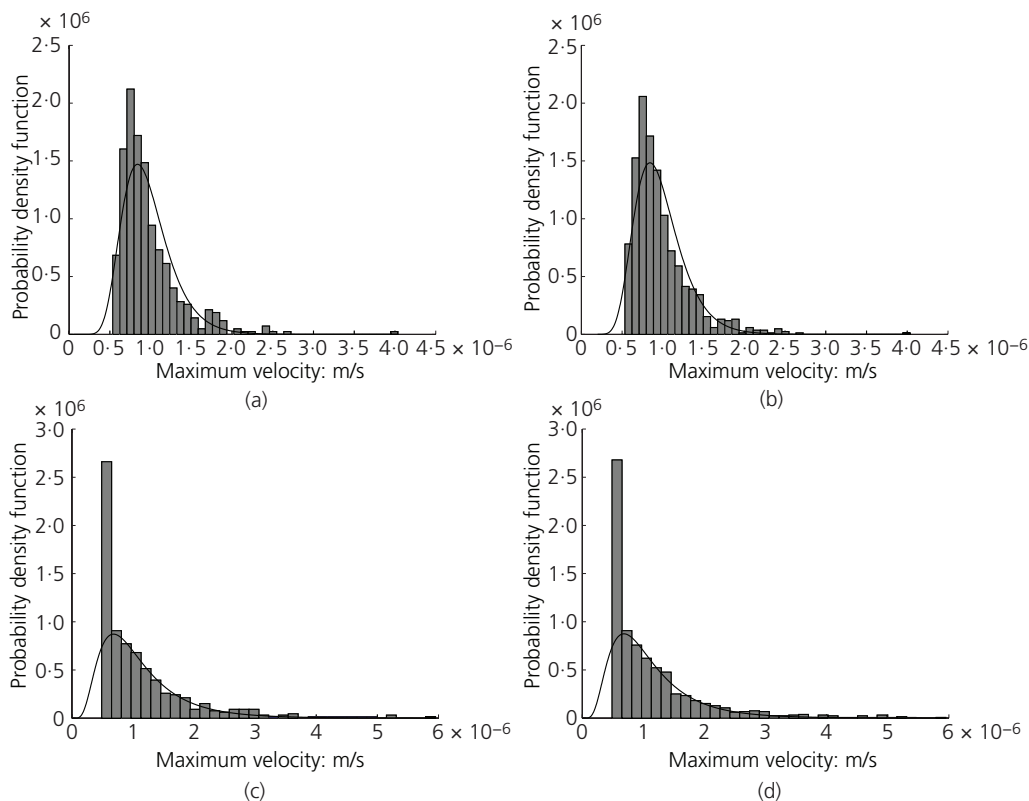| COV	ξ	500 realisations		1000 realisations	
		$\mu_{v_{max}}$: m/s	$\sigma_{v_{max}}$: m/s	$\mu_{v_{max}}$: m/s	$\sigma_{v_{max}}$: m/s
$1 \cdot 0$	1	$0 \cdot 9741 \times 10^{-6}$	$0 \cdot 3663 \times 10^{-6}$	$0 \cdot 9724 \times 10^{-6}$	$0 \cdot 3497 \times 10^{-6}$
	8	$0 \cdot 9412 \times 10^{-6}$	$0 \cdot 3616 \times 10^{-6}$	$0 \cdot 9373 \times 10^{-6}$	$0 \cdot 3609 \times 10^{-6}$
	20	$0 \cdot 9231 \times 10^{-6}$	$0 \cdot 4073 \times 10^{-6}$	$0 \cdot 9143 \times 10^{-6}$	$0 \cdot 3770 \times 10^{-6}$
$6 \cdot 0$	1	$1 \cdot 1338 \times 10^{-6}$	$0 \cdot 6495 \times 10^{-6}$	$1 \cdot 1335 \times 10^{-6}$	$0 \cdot 6189 \times 10^{-6}$
	8	$1 \cdot 1372 \times 10^{-6}$	$0 \cdot 8384 \times 10^{-6}$	$1 \cdot 1343 \times 10^{-6}$	$0 \cdot 8310 \times 10^{-6}$
	20	$1 \cdot 1678 \times 10^{-6}$	$1 \cdot 1687 \times 10^{-6}$	$1 \cdot 1561 \times 10^{-6}$	$1 \cdot 1488 \times 10^{-6}$

Figure 4. Probability density functions of the maximum velocity: (a) 500 realisations, $COV_k = 1·0$ and $\xi = 1$; (b) 1000 realisations, $COV_k = 1·0$ and $\xi = 1$; (c) 500 realisations, $COV_k = 6·0$ and $\xi = 8$; and (d) 1000 realisations, $COV_k = 6·0$ and $\xi = 8$
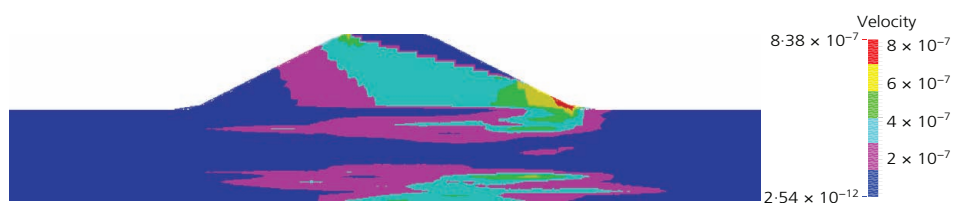

Figure 5. Typical realisation in which the maximum local velocity is close to the slope toe ($COV_k = 1·0$ and $\xi = 20$) (unit: metres per second)
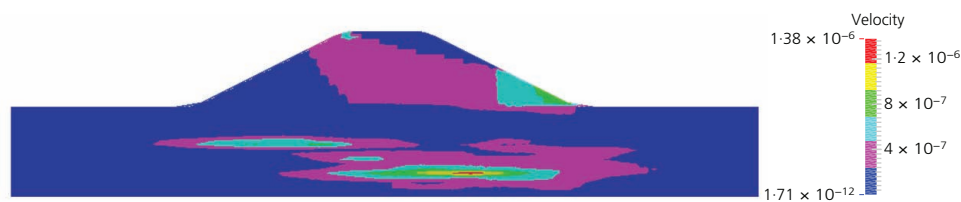

Figure 6. Typical realisation in which the maximum local velocity is near the centre of the foundation ($COV_k = 1·0$ and $\xi = 20$) (unit: metres per second)

different input statistics. However, the value of the maximum local velocity is only one necessary condition for piping. Another factor is the position of the maximum local velocity.

This section investigates the location of the maximum local velocity in all realisations, which is strongly influenced by the variability of the foundation hydraulic conductivity. Among the
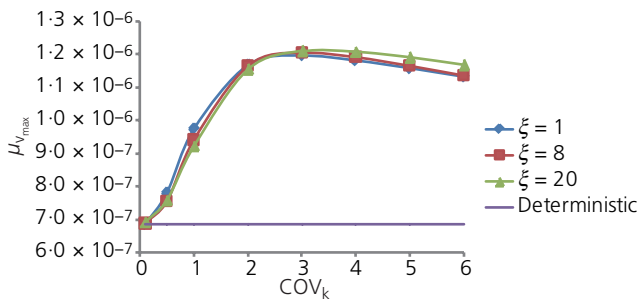
Figure 7. Mean of the maximum local velocity against COV_k of the foundation
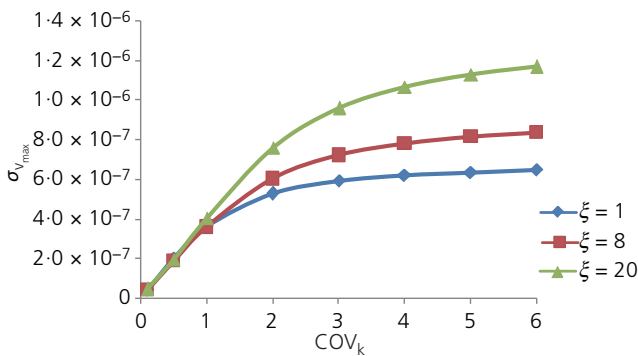

Figure 8. Standard deviation of the maximum local velocity against COV_k of the foundation

realisations, those cases which have the maximum local velocity near the ground surface are more inclined to initiate piping. Therefore, this section highlights several special situations in which different locations of the maximum local velocity are found.
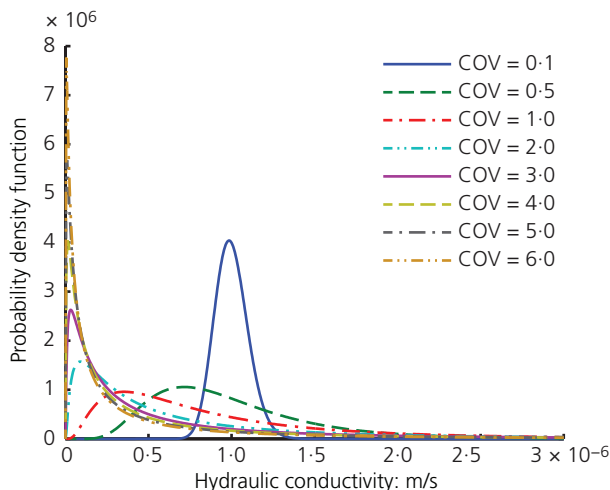
When the COV_k of the foundation hydraulic conductivity is relatively small – for example, $COV_k = 0.1$ – the locations of the maximum local velocity from 500 realisations are found to aggregate into a small area, independent of the degree of anisotropy ξ. This area is located near the downstream slope toe, as seen in Figure 10. In the figure, coloured blocks are used to represent the Gauss points and differently coloured blocks represent the frequency of occurrence of the maximum local velocity from 500 realisations. This aggregation is reasonable considering the small variation of the foundation hydraulic conductivity over the whole domain. When the variation of the foundation hydraulic conductivity is small, the whole field is similar to the homogeneous case. For a homogeneous field, the maximum local velocity is also at the downstream slope toe (as in Figure 10). A simple engineering solution that may be applied in this case is to provide toe protection.

When the COV_k increases to 1.0 and the degree of anisotropy is $\xi = 20$ (or $\xi = 1, 8$), the locations of the maximum local velocity from 500 realisations are more scattered over the domain, as seen in Figure 11, although they are still focused towards the toe. This is due to the significant variation of the foundation hydraulic conductivity in the random fields. Among the 500 realisations, two typical situations can be identified. One is when the maximum local velocity happens close to the ground surface (Figure 5); the other is when the maximum local velocity happens under the dyke (Figure 6). Hence, the location of the maximum local velocity is not as simple to determine as in the situation when COV_k is small. For $COV_k > 1.0$, the spatial distribution of maximum velocity locations is similar to Figure 11, based on 500 realisations.

Figure 5 shows that the maximum local velocity is close to the ground surface, whereas Figure 6 shows that the location of the maximum local velocity may be, in certain cases, far from the ground surface. As already mentioned, piping occurrence can be linked to

Figure 9. Probability density functions of hydraulic conductivity for different COV_k values
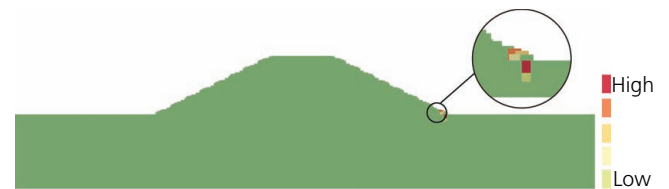

Figure 10. Locations of the points with maximum local velocity from 500 realisations ($COV_k = 0.1$ and $\xi = 1$)

Figure 11. Locations of the points with maximum local velocity from 500 realisations ($COV_k = 1.0$ and $\xi = 20$)

Environmental Geotechnics
Volume 6 Issue EG5

**Probabilistic analysis of seepage for
internal stability of earth embankments**
Liu, Vardon and Hicks

critical hydraulic velocity. In the first situation, it is easier to reach a critical value to initiate piping because the maximum local velocity is near the ground surface. In contrast, in the second situation, it is easier to maintain a passage for piping development once piping has been initiated. This is due to the increasing velocity towards the centre of the foundation. If piping has been initiated near the toe in the second situation, the higher velocity near the centre of the foundation may worsen the situation and promote piping progression.

Exit gradient related to piping initiation

In the previous section, the influence of the spatial variability of hydraulic conductivity on the local velocity distribution has been qualitatively discussed in relation to the maximum local velocity and piping initiation or progression. This section will present a quantitative analysis related to the piping initiation.

Terzaghi (1922) proposed a theoretical criterion to calculate the critical exit gradient i_c for piping initiation. It is valid for internally stable soils (in which the grain size distribution is good) and is defined as

$$2. \quad i_c = (1 - n)\left(\frac{\rho_s - \rho_w}{\rho_w}\right)$$

where n is the porosity and ρ_s and ρ_w are the densities of the soil solids and water, respectively. In most cases, this equation yields
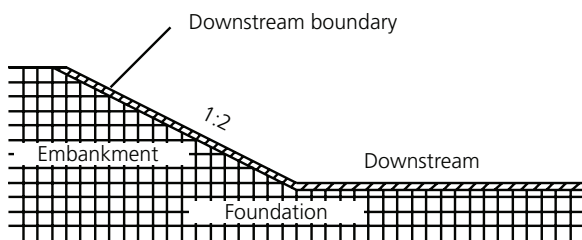
values of i_c around 1·0–1·1. In contrast, Van Beek *et al.* (2014) presented an extensive survey of measured critical exit gradients, based on previous laboratory experiments and field tests related to the study of piping, and reported, in general, lower values of i_c with a larger scatter. However, in the analysis of Van Beek *et al.* (2014), it was pointed out that alongside grain size, porosity and scale, spatial variability could be the cause of the scatter in the experimental results.

The distribution of local water velocity has been considered to be an index to predict piping in previous literature, because it accounts for the combined effect of hydraulic conductivity and hydraulic gradient. Therefore, instead of i_c, the critical local velocity v_c has been used here to predict piping initiation and has been assumed to be derived from i_c and the mean of hydraulic conductivity. Hence, in order to predict piping initiation, the local velocity along the downstream boundary (Figure 12) has been investigated.

In Figure 12, the local velocity in the hatched boundary area is used to predict piping initiation. The maximum local velocity in the hatched area v^b_{max} is compared to the calculated critical velocity v_c and the factor of safety (FOS) relating to piping initiation is defined as

$$3. \quad \text{FOS} = \frac{v_c}{v^b_{max}}$$

where $v_c = \mu_k i_c = 1\cdot0 \times 10^{-6} \times 1\cdot0 = 1\cdot0 \times 10^{-6}$ m/s, in which i_c has been selected to be 1·0 in this example.

Figure 13 shows the probability density function (PDF) and cumulative distribution function (CDF) of the FOS related to piping initiation when $\text{COV}_k = 1\cdot0$ and $\xi = 1$. The vertical solid line in Figure 13(a) indicates the FOS when the foundation is considered to be homogeneous with $k = \mu_k$ – that is, FOS = $1\cdot0 \times 10^{-6}/6\cdot86 \times 10^{-7} = 1\cdot46$. It can be seen that the heterogeneity has a significant influence on the estimation of the FOS. In Figure 13(b), when the
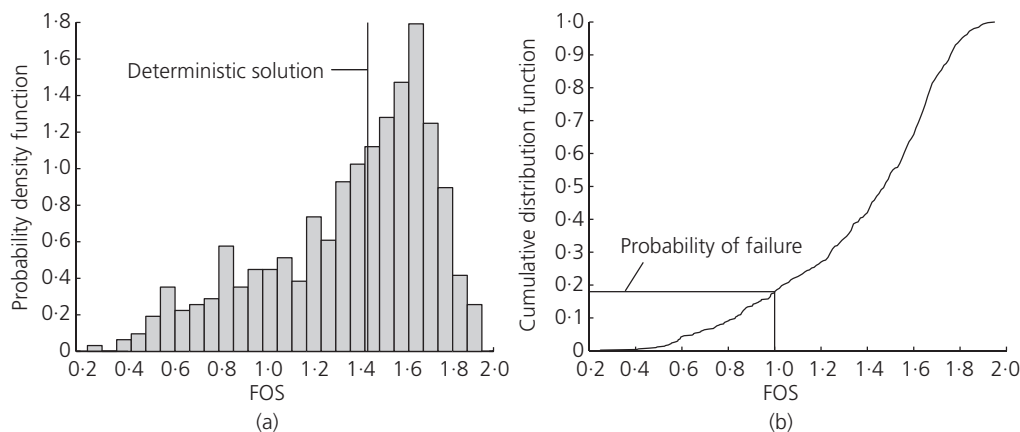

Figure 12. Downstream area relating to piping initiation

Figure 13. PDF and CDF of FOS related to piping initiation ($\text{COV}_k = 1\cdot0$ and $\xi = 1$)

Environmental Geotechnics
Volume 6 Issue EG5

Probabilistic analysis of seepage for
internal stability of earth embankments
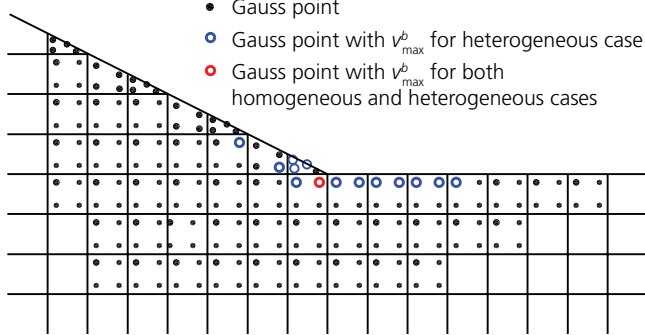Liu, Vardon and Hicks

Figure 14. Close-up of the downstream toe area showing the locations of v^b_{max} as open circles ($COV_k = 1 \cdot 0$ and $\xi = 1$)
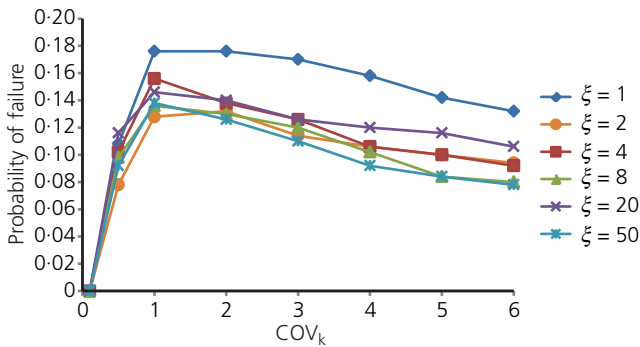

Figure 15. Probability of failure as a function of COV_k and ξ

FOS is smaller than $1 \cdot 0$, it is considered that piping initiation will occur, so that the probability of failure in this case is $17 \cdot 6\%$. Figure 14 shows the comparison of the computed positions of v^b_{max} between the homogeneous and heterogeneous cases. The solid and open circles represent the Gauss points of the FEs, with the red open circle denoting the location of v^b_{max} for the homogeneous case. For the heterogeneous case ($COV_k = 1 \cdot 0$ and $\xi = 1$), the possible locations also include the blue open circles in Figure 14.

Figure 15 summarises the probability of failure as a function of both COV_k and ξ. For all cases, it is found that the probability of failure increases with increasing COV_k when the COV_k is smaller than $1 \cdot 0$ but then decreases for larger values of COV_k. This can be explained based on the results of the previous sections. The reason for the increase is that when COV_k is smaller than $1 \cdot 0$, the maximum local velocity of the whole domain, v_{max}, aggregates in a small area near the downstream slope toe. Specifically, it occurs only at a few Gauss points (see Figure 16(a)); therefore, v_{max} is generally equal to v^b_{max} (relating to the hatched area defined in Figure 12). In addition, the variation of the hydraulic conductivity is limited within a small range when COV_k is small and v_{max} is dominated by the range of the hydraulic conductivity. Because of these two reasons, when COV_k increases from $0 \cdot 1$ to $1 \cdot 0$, the range of the hydraulic conductivity becomes larger so that it causes a higher maximum local velocity over the whole domain, which is the reason for the increase of v^b_{max}. The increase of v^b_{max} causes the increase in the probability of failure.

When COV_k is greater than $1 \cdot 0$, the location of v_{max} is scattered throughout the whole foundation. Meanwhile, there is no
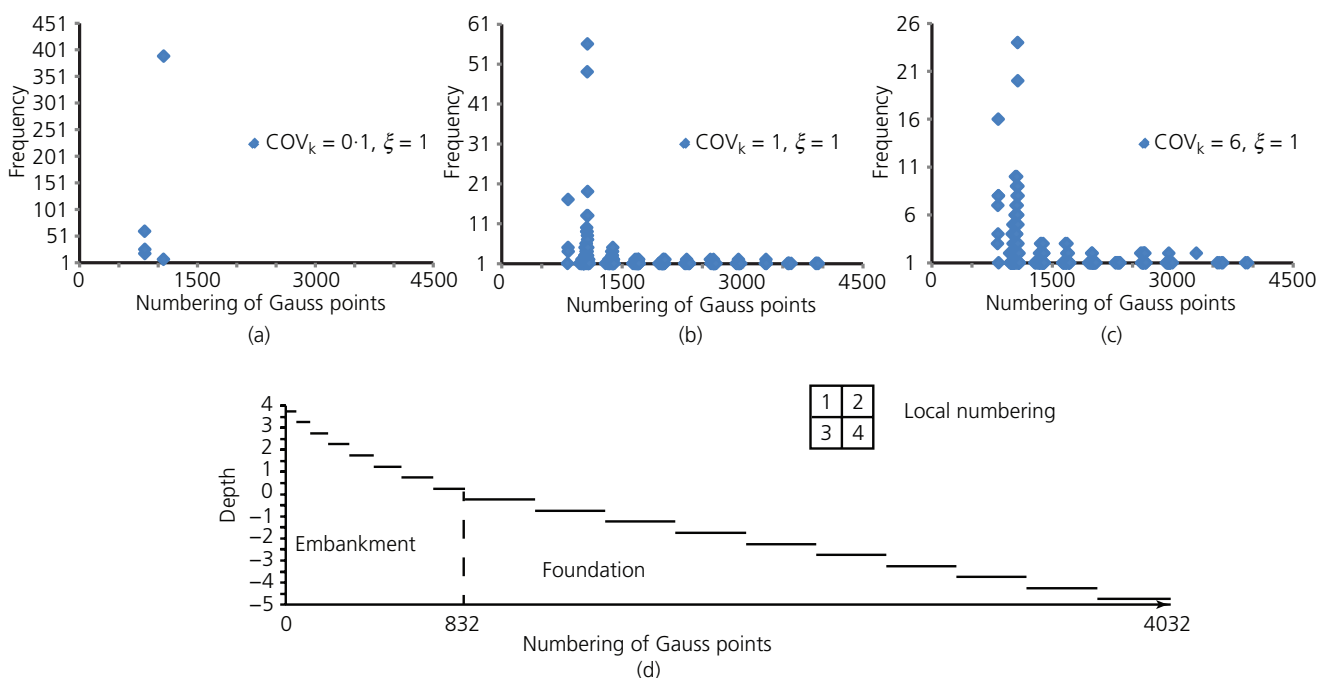

Figure 16. Frequency and locations of Gauss points with v_{max} for different COV_k values

Environmental Geotechnics
Volume 6 Issue EG5

**Probabilistic analysis of seepage for
internal stability of earth embankments**
Liu, Vardon and Hicks

significant change in the mean of v_{max} when COV_k is greater than 1·0 (Figure 7). However, the scattering is much more obvious with the increase of COV_k (see Figures 16(b) and 16(c)), which leads to a smaller v_{max}^b. Due to this reduction, the probability of failure initiation decreases when COV_k is greater than 1·0.

In Figure 15, there is no obvious tendency for a variation in the probability of failure with the degree of anisotropy for anisotropic cases, although there is a difference between the isotropic ($\xi = 1$) and anisotropic cases – that is, there is a reduction when $\xi > 1$. The reason for the difference between isotropic and anisotropic cases may be that for anisotropic fields, there could be preferential horizontal flow which would reduce the local velocity upwards. However, Figure 15 shows negligible difference between the anisotropic analyses, possibly because of v_{max}^b being studied only in a thin layer of elements at the downstream boundary and the degree of anisotropy affecting the distribution of the hydraulic conductivity over the whole foundation. Fenton and Griffiths (2008) also found that the exit hydraulic gradient of a water-retaining structure shows no clear variation with the scale of fluctuation of the hydraulic conductivity (for their analyses based on isotropic spatial variability).

Influence of heterogeneity on the kinetic energy of seepage

Richards and Reddy (2014) proposed a method which uses the kinetic energy to predict the initiation of piping. In this section, the influence of the heterogeneity on the kinetic energy is investigated.

The local kinetic energy of the water, E_1, is defined as

$$4. \quad E_1 = \frac{1}{2} M_f v_s^2$$

where M_f is the mass of fluid and v_s is the pore seepage velocity. The v_s is calculated from the computed Darcy flow velocity v.

$$5. \quad v_s = \frac{q}{A_p} = \frac{vA}{A_p} = \frac{v}{n}$$

where q is the discharge, A_p is the area of the voids in the cross-section and A is the total area of the cross-section.
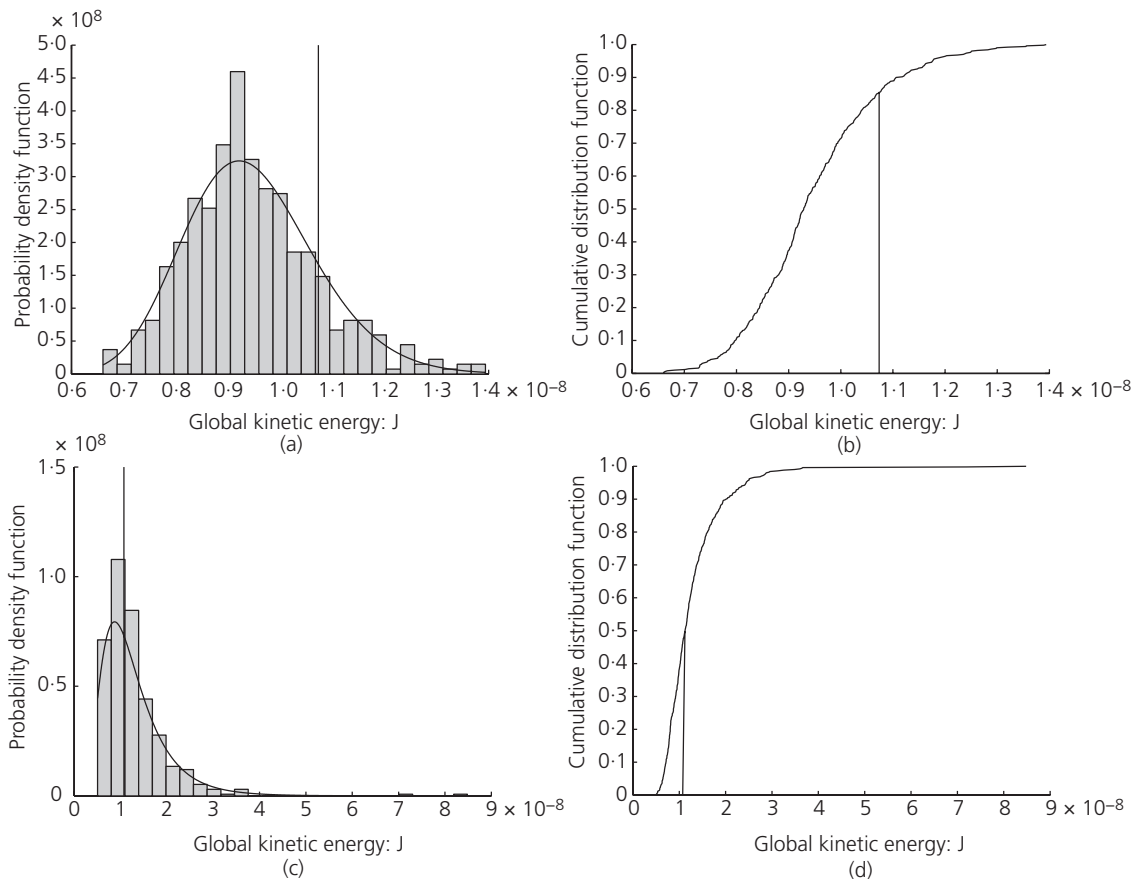

Figure 17. PDF and CDF values of E_g: (a) PDF for $COV_k = 1·0$ and $\xi = 1$, (b) CDF for $COV_k = 1·0$ and $\xi = 1$, (c) PDF for $COV_k = 1·0$ and $\xi = 20$ and (d) CDF for $COV_k = 1·0$ and $\xi = 20$

Environmental Geotechnics
Volume 6 Issue EG5

Probabilistic analysis of seepage for
internal stability of earth embankments
Liu, Vardon and Hicks

Equations 4 and 5 can be combined as

6.
$$E_1 = \frac{1}{2}M_f v_s^2 = \frac{1}{2}\rho_w V n \left(\frac{v}{n}\right)^2 = \frac{1}{2}\rho_w V \frac{v^2}{n}$$

where V is the volume of soil and since it is a 2D plane strain problem, $V = A$. The global kinetic energy E_g is the integral of E_1 across the domain.

In Figure 17, the PDF and CDF values of E_g when $COV_k = 1\cdot0$ and $\xi = 1, 20$, are shown. The vertical solid line indicates the value of E_g when the foundation is homogeneous – that is $E_{g,homo} = 1\cdot07 \times 10^{-8}$ J. Figure 17 shows that the heterogeneity of the hydraulic conductivity can result in a larger global energy compared to that of the homogeneous case. In addition, the largest

value in the distribution can be significantly larger than the smallest value.

Figure 18 shows the spatial distribution of E_1 for the homogeneous case, whereas Figure 19 shows the realisation of the E_1 and the corresponding random field of hydraulic conductivity, for the realisation (out of 500) for which E_g is the maximum (for both sets
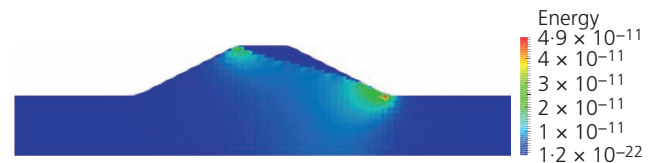

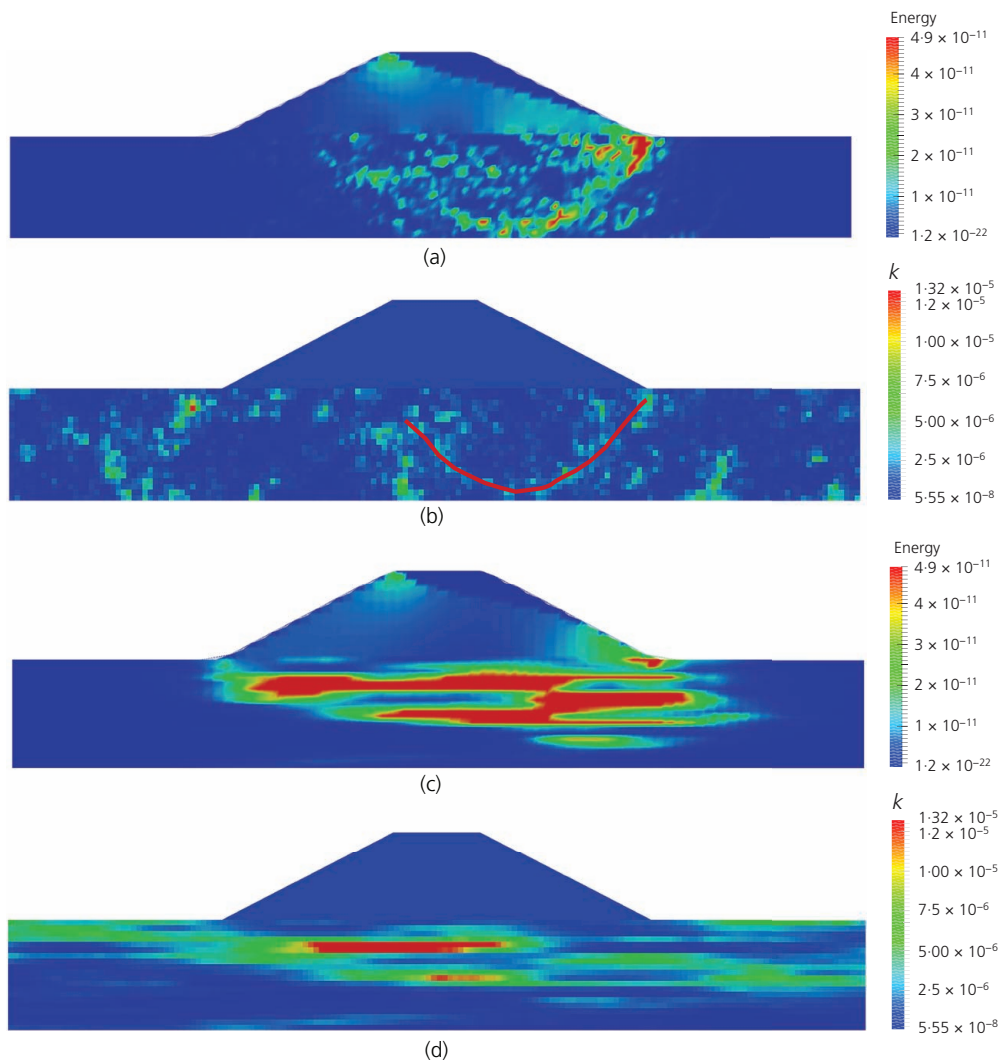**Figure 18.** Distribution of E_1 for homogeneous case (unit: Joules)

Figure 19. Realisation with the maximum global kinetic energy for $COV_k = 1\cdot0$ and $\xi = 1$ ((a) and (b)) and $COV_k = 1\cdot0$ and $\xi = 20$ ((c) and (d)): (a) kinetic energy (unit: Joules), (b) hydraulic conductivity (unit: metres per second), (c) kinetic energy (unit: Joules) and (d) hydraulic conductivity (unit: metres per second)
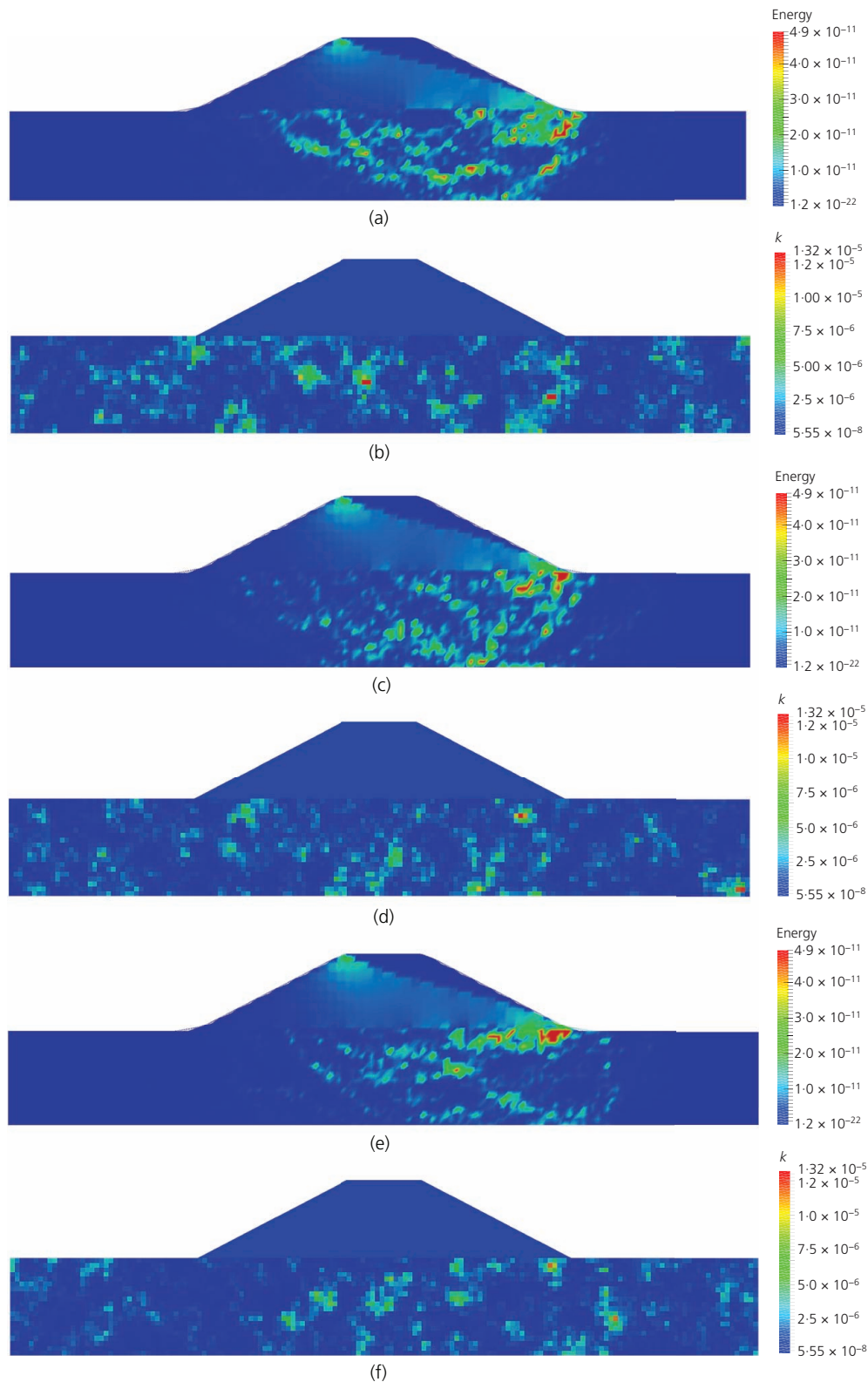
Environmental Geotechnics
Volume 6 Issue EG5

**Probabilistic analysis of seepage for
internal stability of earth embankments**
Liu, Vardon and Hicks

Figure 20. Realisations with high global kinetic energy for $COV_k = 1.0$ and $\xi = 1$: (a) second highest (unit: Joules), (b) hydraulic conductivity (unit: metres per second), (c) fifth highest (unit: Joules), (d) hydraulic conductivity (unit: metres per second), (e) tenth highest (unit: Joules) and (f) hydraulic conductivity (unit: metres per second)
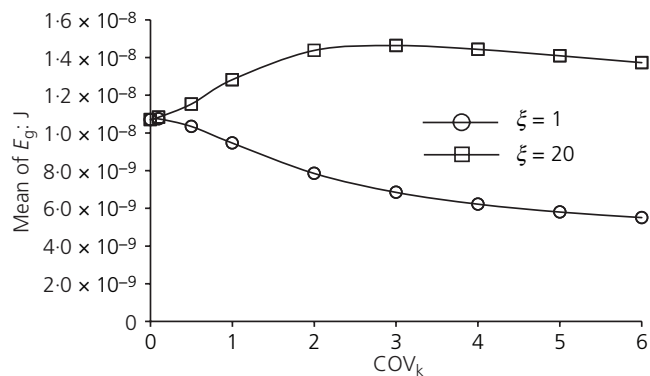
Environmental Geotechnics
Volume 6 Issue EG5

Probabilistic analysis of seepage for
internal stability of earth embankments
Liu, Vardon and Hicks

Figure 21. Mean of E_g against COV_k for different degrees of anisotropy

of input statistics illustrated in Figure 17). It can be seen from the hydraulic conductivity field, in Figure 19(b), that the higher local hydraulic conductivity forms a passage of preferential flow (indicated by the red line) which generates higher E_1 (Figure 19(a)). For comparative purposes, Figure 20 shows similar results for three other realisations when $COV_k = 1·0$ and $\xi = 1$, corresponding to E_g being the second, fifth and tenth largest among the 500 realisations. In Figure 19(d), the higher local hydraulic conductivity at the centre of the foundation causes the higher E_1 at the centre (Figure 19(c)). A comparison between Figures 18 and 19 shows that the heterogeneity of the hydraulic conductivity not only increases the value of the E_1, but also influences its spatial distribution significantly. In addition, it can be seen that the area of high E_1 in the heterogeneous foundation is larger than that in the homogeneous foundation, particularly for the larger value of ξ.

The results in Figures 17 and 19 show that for a higher degree of anisotropy, the global kinetic energy is likely to increase and the connected zones are also likely to increase, which increases the likelihood of piping to grow if initiated.

Figure 21 shows the variation of the mean of E_g against COV_k for $\xi = 1, 20$. For $\xi = 1$, the figure shows that the mean of E_g decreases with an increase in COV_k, whereas for $\xi = 20$, the mean of E_g generally increases with an increase in COV_k. An increase in COV_k means more low values of hydraulic conductivity (see Figure 9). For a relatively small scale of fluctuation in all directions (in this case, represented by $\xi = 1$), it is more difficult for the flowing water to avoid less permeable zones. This leads to a decrease in the mean velocity and, therefore, to a lower global kinetic energy. For a high level of anisotropy ($\xi = 20$), a more layered appearance occurs in the soil and flow is increasingly able to focus in almost continuous 'layers' of high hydraulic conductivity. This leads to a greater velocity and, therefore, to a higher kinetic energy. The reduction in the mean of E_g from a peak at around $COV_k = 3$ is due to less high values of hydraulic conductivity at higher values of COV_k, as discussed in the section headed 'Probabilistic analysis of seepage in and under an embankment' in relation to Figure 7.

Conclusion

The influence of spatial variability, in the foundation hydraulic conductivity, on the local seepage velocity through and beneath an embankment has been investigated. A number of features known to influence the internal stability were examined – that is, local velocity, hydraulic gradient and kinetic energy. It has been shown that when the foundation is only weakly heterogeneous, it is easy to narrow down the zone in which piping may initiate. The maximum local velocity occurs in a small area close to the downstream slope toe, and toe protection could be installed. However, when the foundation shows strong heterogeneity in hydraulic conductivity, the problem becomes more complex due to the significant variation of the maximum local velocity over the domain. Generally, this variation can be categorised into two types.

- The maximum local velocity is located under the foundation, far from the downstream ground surface. The high local velocity zone is surrounded by lower velocity zones. It is easier to form a passage for piping development once piping is initiated due to a higher drag force.
- The maximum local velocity occurs near the downstream ground surface. It is easier to reach critical conditions to initiate piping.

In the quantitative analyses of the exit gradient and kinetic energy related to piping initiation, it was found that the heterogeneity of hydraulic conductivity increased the possibility of piping initiation. Due to the heterogeneity, the exit velocity gradient is generally higher than that of the homogeneous case. Meanwhile, in the computation of kinetic energy, it was found that the global kinetic energy E_g could also be higher than that of the homogeneous case and the distribution of the local kinetic energy E_1 was significantly different from the homogeneous case. In addition, E_g decreases with an increase in COV_k; in particular, high values of degree of anisotropy lead, in general, to higher global levels of kinetic energy and pathways of locally elevated kinetic energy, which, in turn, lead to an increased risk of piping growth (once initiated). Further studies are needed to investigate further the significance of the processes outlined here and to include the effects of local behaviour into assessment methods.

Acknowledgements

REFERENCES

Bathe KJ and Khoshgoftaar MR (1979) Finite element free surface seepage analysis without mesh iteration. *International Journal for Numerical and Analytical Methods in Geomechanics* **3(1)**: 13–22, http://dx.doi.org/10.1002/nag.1610030103.

Bligh WG (1910) Dams, barrages and weirs on porous foundations. *Engineering News* **64(26)**: 708–710.

Environmental Geotechnics
Volume 6 Issue EG5

Probabilistic analysis of seepage for
internal stability of earth embankments
Liu, Vardon and Hicks

Chapuis RP and Aubertin M (2001) A simplified method to estimate
saturated and unsaturated seepage through dikes under steady-state
conditions. *Canadian Geotechnical Journal* **38(6)**: 1321–1328, http://
dx.doi.org/10.1139/cgj-38-6-1321.

Chapuis RP, Chenaf D, Bussière B, Aubertin M and Crespo R (2001) A
user's approach to assess numerical codes for saturated and
unsaturated seepage conditions. *Canadian Geotechnical Journal* **38(5)**:
1113–1126, http://dx.doi.org/10.1139/cgj-38-5-1113.

Duncan JM (2000) Factors of safety and reliability in geotechnical
engineering. *Journal of Geotechnical and Geoenvironmental
Engineering* **126(4)**: 307–316, http://dx.doi.org/10.1061/(ASCE)1090-
0241(2000)126:4(307).

Fenton GA and Griffiths DV (1996) Statistics of free surface flow through
stochastic earth dam. *Journal of Geotechnical Engineering* **122(6)**:
427–436, http://dx.doi.org/10.1061/(ASCE)0733-9410(1996)122:6
(427).

Fenton GA and Griffiths DV (2008) *Risk Assessment in Geotechnical
Engineering*. Wiley, Hoboken, NJ, USA.

Fenton GA and Vanmarcke EH (1990) Simulation of random fields via
local average subdivision. *Journal of Engineering Mechanics* **116(8)**:
1733–1749, http://dx.doi.org/10.1061/(ASCE)0733-9399(1990)116:8
(1733).

Foster M, Fell R and Spannagle M (2000) A method for assessing the
relative likelihood of failure of embankment dams by piping.
Canadian Geotechnical Journal **37(5)**: 1025–1061, http://dx.doi.org/
10.1139/t01-109.

Griffiths DV and Fenton GA (1993) Seepage beneath water retaining
structures founded on spatially random soil. *Géotechnique* **43(4)**:
577–587, https://doi.org/10.1680/geot.1993.43.4.577.

Hicks MA and Samy K (2004) Stochastic evaluation of heterogeneous
slope stability. *Italian Geotechnical Journal* **38(2)**: 54–66.

Lane EW (1935) Security from under-seepage-masonry dams on earth
foundations. *Transactions of the American Society of Civil Engineers*
100(1): 1235–1272.

Le TMH, Gallipoli D, Sanchez M and Wheeler SJ (2012) Stochastic
analysis of unsaturated seepage through randomly heterogeneous earth
embankments. *International Journal for Numerical and Analytical
Methods in Geomechanics* **36(8)**: 1056–1076, http://dx.doi.org/10.
1002/nag.1047.

Li Y, Hicks MA and Vardon PJ (2016) Uncertainty reduction and sampling
efficiency in slope designs using 3D conditional random fields.
Computers and Geotechnics **79**: 159–172, http://dx.doi.org/10.1016/j.
compgeo.2016.05.027.

Liu K (2017) *Reduction of Uncertainty in Stability Calculations for Slopes
under Seepage.* PhD thesis, Delft University of Technology, Delft,
the Netherlands.

Liu K, Vardon PJ and Hicks MA (2017) Combined effect of hysteresis and
heterogeneity on the stability of an embankment under transient
seepage. *Engineering Geology* **219**: 140–150, http://dx.doi.org/10.
1016/j.enggeo.2016.11.011.

Lloret-Cabot M, Hicks MA and van den Eijnden AP (2012) Investigation of
the reduction in uncertainty due to soil variability when conditioning a
random field using Kriging. *Géotechnique Letters* **2(3)**: 123–127,
https://doi.org/10.1680/geolett.12.00022.

Richards KS and Reddy KR (2012) Experimental investigation of initiation
of backward erosion piping in soils. *Géotechnique* **62(10)**: 933–942,
https://doi.org/10.1680/geot.11.P.058.

Richards KS and Reddy KR (2014) Kinetic energy method for predicting
initiation of backward erosion in earthen dams and levees.
Environmental and Engineering Geoscience **20(1)**: 85–97, http://dx.
doi.org/10.2113/gseegeosci.20.1.85.

Sellmeijer JB (2006) Numerical computation of seepage erosion below
dams (piping). *Proceedings of the 3rd International Conference on
Scour and Erosion, Amsterdam, the Netherlands*, pp. 596–601.

Sellmeijer JB and Koenders MA (1991) A mathematical model for piping.
Applied Mathematical Modelling **15(11)**: 646–651, http://dx.doi.org/
10.1016/S0307-904X(09)81011-1.

Sivakumar Babu GL and Vasudevan AK (2008) Seepage velocity and
piping resistance of coir fiber mixed soils. *Journal of Irrigation and
Drainage Engineering* **134(4)**: 485–492, http://dx.doi.org/10.1061/
(ASCE)0733-9437(2008)134:4(485).

Smith IM, Griffiths DV and Margetts L (2013) *Programming the Finite
Element Method*. Wiley, Hoboken, NJ, USA.

Terzaghi K (1922) Der Grundbruch an Stauwerken und seine Verhütung.
Die Wasserkraft **17(24)**: 445–449 (in German). Reprinted in Terzaghi
K (1960) *From Theory to Practice in Soil Mechanics*. Wiley,
Hoboken, NJ, USA, pp. 114–118.

Van Beek VM, Bezuijen A, Sellmeijer JB and Barends FBJ (2014) Initiation
of backward erosion piping in uniform sands. *Géotechnique* **64(12)**:
927–941, https://doi.org/10.1680/geot.13.P.210.

Vardon PJ, Liu K and Hicks MA (2016) Reduction of slope stability
uncertainty based on hydraulic measurement via inverse analysis.
*Georisk: Assessment and Management of Risk for Engineered Systems
and Geohazards* **10(3)**: 223–240, http://dx.doi.org/10.1080/17499518.
2016.1180400.

Wang B, Hicks MA and Vardon PJ (2016) Slope failure analysis using
the random material point method. *Géotechnique Letters* **6(2)**:
113–118, https://doi.org/10.1680/jgele.16.00019.

Zhu H, Zhang LM, Zhang LL and Zhou CB (2013) Two-dimensional
probabilistic infiltration analysis with a spatially varying permeability
function. *Computers and Geotechnics* **48**: 249–259, http://dx.doi.org/
10.1016/j.compgeo.2012.07.010.

How can you contribute?

To discuss this paper, please submit up to 500 words to
the editor at journals@ice.org.uk. Your contribution will be
forwarded to the author(s) for a reply and, if considered
appropriate by the editorial board, it will be published as a
discussion in a future issue of the journal.